ECS Transactions, 64 (2) 17-28 (2014)
10.1149/06402.0017ecst ©The Electrochemical Society

A Study of SOFC Cathode Degradation in H_2O Environments

C. Pellegrinelli, Y.-L. Huang, J. A. Taillon, L. G. Salamanca-Riba, and E. D. Wachsman

Department of Materials Science and Engineering, University of Maryland, College Park, MD, 20742

An understanding of degradation mechanisms of SOFC cathodes under operating conditions is essential for the development of commercial, intermediate temperature (<700°C) SOFCs. Literature shows that the presence of H_2O in the cathode impacts the performance of SOFCs. In this study, we attempt to determine the degradation mechanisms of the composite cathode, $(La_{0.8}Sr_{0.2})_{0.95}MnO_{3\pm\delta}$ - $(Y_2O_3)_{0.8}(ZrO_2)_{0.92}$ (LSM-YSZ) in an H_2O environment based on a multi-faceted approach. LSM-YSZ/YSZ/LSM-YSZ symmetric cells were examined in the presence of the contaminant (H_2O) under different cycling, polarization and working conditions. Symmetric cell performance was measured by *in-situ* electrochemical impedance spectrometry (EIS), and directly compared to quantitative microstructural parameters obtained from FIB-SEM 3D reconstructions. FIB-SEM is a powerful technique to quantify important performance characteristics such as triple phase boundary (TPB) length and surface to volume ratio. EIS and FIB-SEM results were compared to kinetic rate data, extracted from isotope exchange experiments, to determine mechanistic relationships.

Introduction

Solid oxide fuel cells (SOFC) are a promising technology for the conversion of hydrocarbon fuels (H_2, CH_4, etc.) directly to electricity through the electrochemical oxidation of the fuel, with an efficiency of up to >50%. Among all the electrochemical reactions in SOFCs, the reduction of oxygen molecules on the cathode corresponds to the majority of the polarization loss. The selection of a proper catalyst for the cell cathode is important, and ABO_3 perovskite materials have been proven to be an effective catalyst for the oxygen reduction reaction (ORR) (1-3). Through the selection of different A and B site cations, characteristics such as conductivity (electronic and ionic), phase stability, catalytic activity, and thermal expansion coefficients (TEC) can be altered, which can be matched to an ion conducting electrolyte, such as yittria stabilized zirconia $(Y_2O_3)_{0.8}(ZrO_2)_{0.92}$ (YSZ). $(La_{0.8}Sr_{0.2})_{0.95}MnO_{3\pm\delta}$ (LSM) has been studied extensively due to its exceptional performance and stability as a cathode material, and is the current choice for commercial SOFCs (4). The doping of Sr(2+) in the La(3+) sites creates a charge imbalance creating mixture of valance states of Mn pairs resulting in the high catalytic activity toward the ORR. Due to the catalytic nature of perovskite cathode materials, the high operating temperatures of fuel cells, and the unavoidable presence of other gasses on the air side of the cell, we expect some unwanted interactions to occur.

Although there has been significant effort already in improving the performance of SOFCs there remain issues with degradation of the electrode materials. In particular, degradation of the cathode can cause high polarization losses, accounting for significant decreases in efficiency. In order to improve the cathode durability, it's essential to separate the various contributions to degradation; physical (cracking, delamination, coarsening), chemical (secondary phase formation, segregation), catalytic (blocking or poisoning of surface sites). It has been show in literature that H_2O and CO_2 in the air can have a large impact on the durability and performance of the cathode (5-7). In order to improve the stability of the SOFC cathode in common air contaminants we need to understand the fundamentals that govern the oxygen reduction reaction (ORR) occurring at the cathode surface. Subsequently, with this knowledge, we can begin to design materials system that will improve the stability of the SOFC cathode.

In this work, we investigate the degradation effects of H_2O on LSM-YSZ composite cathodes. The degradation is studied under both open circuit (OC) and applied bias conditions to determine how an external driving potential may enhance or prevent unwanted reactions of H_2O with the ORR catalyst.

Based on *in-situ* electrochemical impedance spectroscopy (EIS) measurements on a symmetrical cell in a controlled contaminant environment, we can probe the interaction between H_2O and the composite cathode (8-10). The *in-situ* cell testing results are compared with post analysis FIB-SEM 3D reconstructions (11-17) and kinetic rate data extracted from isotope exchange experiments (18-21). A multifaceted approach is necessary to separate the effects of contaminants, such as coarsening of the microstructure, formation of secondary phases and changes of the materials surface characteristics. The results show that H_2O affects cell performance and that polarization may exacerbate these effects.

Experimental

In order to investigate the effects of H_2O degradation on LSM-YSZ composite cathodes using impedance spectroscopy, symmetrical button cells were created. The electrolyte support for these cells was fabricated using the tape casting method to achieve high grain density and uniform thickness. 8YSZ powder (TOSOH Corp.) was mixed with ethanol, toluene, polyvinyl butyral (PVB) and butyl benzyl phthalate (BBP), and balled milled for 48 hours to form a uniform slurry. After ball milling the slurry was filtered and de-aired under vacuum for 2-4 hours to remove any bubbles that potentially formed during the milling process. The de-aired slurry was then tape casted and dried at 120°C for 6-8 hours. Tapes of approximately 180μm thickness (after drying) were formed. In order to increase the thickness of the electrolyte, four layers of tape were laminated together using a hot press at 180°C and a pressure of 1.5 metric tons for 10 minutes. The laminated tape was then punched with a 1.25 inch die and pre-sintered at 900°C for two hours. The pre-sintered bodies were subsequently sintered at 1450°C between two alumina discs for 5 hours to obtain dense, flat, uniform electrolytes. The sintered YSZ button cells were approximately 450μm in thickness and 1 inch in diameter. Composite cathode slurries, 50-50 wt.% LSM-YSZ (Fuel Cell Materials), were screen printed onto both sides of the YSZ electrolyte support to ensure uniform thickness, and symmetry regarding size and placement. A drawing of the symmetrical LSM-YSZ/YSZ/LSM-YSZ cell configuration is shown in Fig. 1(b). This specific design was used to enable accurate measurements for both two and three electrode designs.

Impedance Spectroscopy Measurements

Impedance spectroscopy measurements were performed using a 1455 Cell Test System (Solartron Analytical). The reactor used for testing the symmetrical cells, shown schematically in Fig. 1(a), was specifically designed to meet the requirements of our experiments. Alumina tubes (99.5% purity) are used to separate gas flows for the working and counter electrodes, physical support of the cell, and provide support for electrical contact wires connecting to pieces of gold microgrid. This gold microgrid has been cut to match the cathode pattern that is screen printed on the symmetric cells. In order to maintain contact between the mesh and the cathode a highly porous gas diffuser, machined from reticulated alumina, has been inserted between the alumina tubes and the gold mesh. The reticulated alumina uses the weight of the tubes to put pressure on the gold microgrid, to maintain electrical contact with the composite cathode surface during electrical measurements. Under three-electrode measurement settings a platinum point reference can be inserted and placed in the center of electrolyte. Swagelok UltraTorr fittings are connected to the alumina tubes to provide access for the gas environments to be tested in. Consideration has been made to create a reactor that will minimize the effects of cell preparation, such as the painting of precious metal pastes to attach wire mesh contacts to the surface of the cathode.

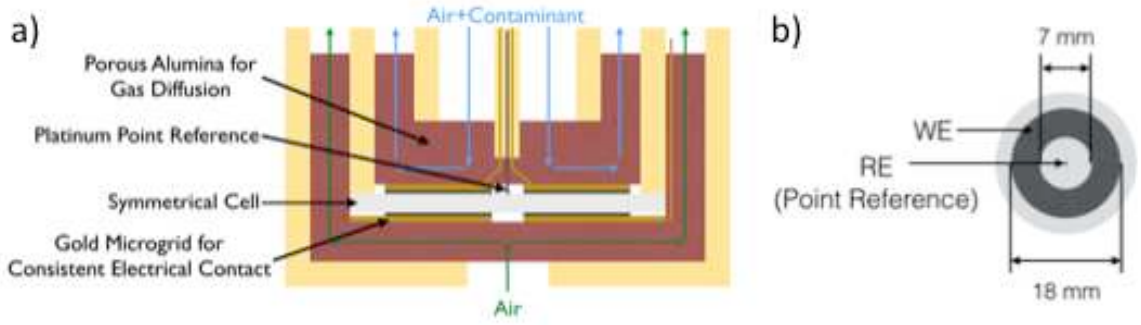

Figure 1. (a) Schematic of active region in a two-environment button cell test reactor. Highly porous reticulated alumina supports are used to keep gold micro-grid in contact with symmetrical cell electrodes, while allowing gas to diffuse freely to the cell surface. (b) A representation of one side of a symmetrical cell, where cathode paste is screen-printed in a 'doughnut' pattern on both sides of the electrolyte support. A simple Pt point reference can be used for 3-electrode measurements.

Impedance spectroscopy measurements were taken for LSM-YSZ/YSZ/LSM-YSZ symmetrical button cells under polarization and moisture conditions for a period of 500 hours. The conditions for the cell during aging consisted of synthetic air with a total flow rate of 100 SCCM of N_2-O_2 gas mixtures. On the working electrode (WE) side, separated from the counter electrode (CE), the synthetic air was bubbled through water using a quartz glass impinger, with the water in the container being held at a constant temperature of ~25°C to generate a 3% H_2O moisture environment into the cell testing system. During polarization, a voltage of -0.7V was applied across the cell (from WE to CE), in order to drive oxygen ions from the WE to the CE, as would take place in an operating SOFC. The aging process was set up to monitor the effects of polarization on the cell under an H_2O environment, with respect to how the same cell operated under open circuit conditions. As such, a voltage of -0.7V was applied across the cell for two hours, followed by an impedance measurement with a -0.7V DC offset. Subsequently,

there was a two-hour period of open circuit (OC) conditions, followed by an impedance measurement with no DC offset (again OC). As such we were able to measure the resistance of the cell for 500 hours in H_2O under alternating polarization and OC conditions to draw a clearer picture of what effects if any, become more apparent in the presence of both H_2O and an applied bias.

Results and Discussion

LSM-YSZ/YSZ/LSM-YSZ Symmetric Cell in H_2O

Figure 2(c) shows a plot of the resistance of an LSM-YSZ/YSZ/LSM-YSZ symmetrical cell during aging under an 80-20 mixture of N_2-O_2 that is bubble through water held at 25°C. Impedance data has been fit according to the equivalent circuit shown in Fig. 2(a), as shown in Fig. 2(b). Figure 2(c) shows a clear trend in the polarization resistance, in which the value of the secondary low frequency arc R_2 increases between 0 and 14 hours of aging in an H_2O environment. The value of R_2 then decreases between 14 and 48 hours. Subsequently, the cell was aged for 380 total hours before post-mortem FIB-SEM analysis.

After 380 hours, the LSM-YSZ cathode on the air + 3% H_2O side had visible discoloration, while the dry air-side showed no discoloration. The discoloration indicates that air + 3% H_2O causes degradation of cells, without any bias. To further study the degradation of the composite LSM-YSZ cell in water contamination conditions, similar *in-situ* isotope exchange tests were perform on LSM powders. To directly compare with the cell testing results in Fig. 2(a), isothermal isotope exchange (IIE) of LSM powder was performed after aging at same operating temperature (800°C) in the same concentration of contaminant (3% H_2O) for the same amount of time that was confirmed by EIS to have different degradation processes, i.e. 0 hours, 14 hours, and 48 hours. Effects of aging time on the accumulated ^{18}O exchange curves obtained from IIE of LSM in H_2O are shown in Fig. 2(d). The concentration of scrambled product $^{16}O^{18}O$ is seen to decrease from 0 to 14 hours and then increase again from 14 to 48 hours.

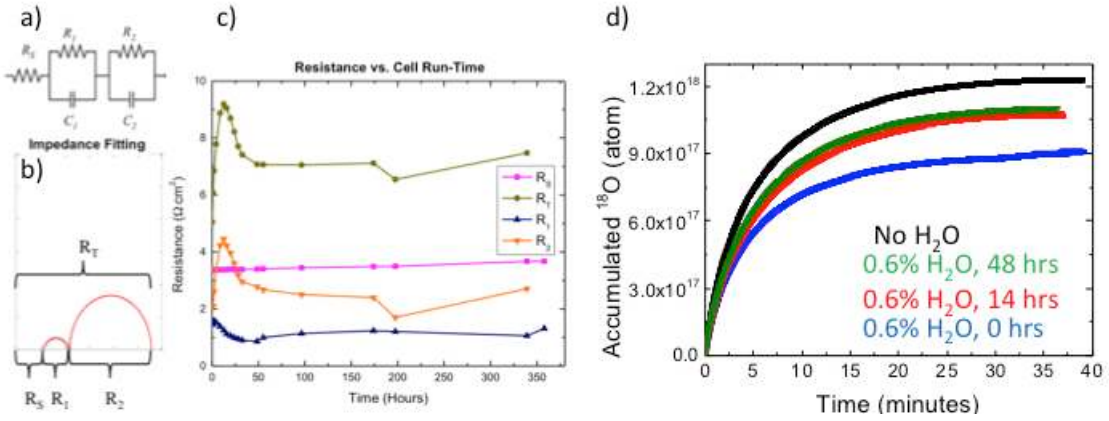

Figure 2. Correlation between *in*-situ EIS measurements and powder isotope exchange experiment in the present of H_2O: (a) the equivalent circuit for EIS data and the fitting parameters for each arc, (b) the resistances as a function of aging time and (c) the accumulated 18O curve calculated from the IIE experiments as a function of aging time

Comparison to Isotope Exchange Data. A direct comparison of cell testing and powder testing results is shown in Fig. 2. The accumulated ^{18}O curve was calculated by considering the difference of mass $^{18}O^{18}O$ flowing into and out the system:

$$M(t) = 2*\text{Total Oxygen} - \{2*(^{36}O_2) + {}^{34}O_2\} - \{H_2{}^{18}O)\} \quad [1]$$

Where M(t) is the total accumulated ^{18}O exchange to the lattice at time (t). The accumulated ^{18}O curves in Fig. 2(d) are based on IIE at 800°C in 0.3% H_2O and it shows change of total ^{18}O into lattice at different aging times. Importantly, cell testing and IIE results show similar trends, indicating change in the oxygen reduction reaction (ORR), determined by IIE, is responsible for change in impedance. The exchange flux changed as a function of aging time and cannot be fitted with one single first order reaction model. A two-parallel exchange model is proposed to explain the difference of the exchange flux from the linear driving force of isotope concentration gradient, assuming there are two parallel pathways for oxygen surface exchange (22-24):

$$C = C_1 e^{-k_1 t} + C_2 e^{-k_2 t} \quad [2]$$

The surface exchange coefficients (k_1 and k_2) denote the fast and slow transport path, respectively. C_1 and C_2 are the available surface sites for each of the reaction path. The fast oxygen surface exchange coefficient seems to have positive correlated to the aging in H_2O, while the slow oxygen surface exchange coefficients show a relative insensitive to the present of H_2O. The details of the isotope exchange experiments are currently being analyzed.

FIB-SEM and TEM Analysis. FIB-SEM analysis was performed as previously reported (25). TEM images were collected on an FEI Titan™ G2 80-200 ChemiSTEM, courtesy of FEI Company. The plot of phase volume fraction obtained by FIB-SEM 3D reconstruction as a function of distance from cathode/electrolyte interface is shown Fig. 3. The influence of aging on phase distribution can be clearly seen in each sample with different aging environment. The aged samples show a greater variability, and are summarized in Table I. The results can be directly compared with the *in-situ* EIS measurements, which show an increasing of polarization resistance after 500 hours aging time. The coarsening of the microstructure and the presence of the inter-diffusion between LSM and YSZ, which can be observed by FIB-SEM, could be responsible for the change in impedance spectra.

TABLE I. Variability in phase fraction for LSM-YSZ composite cathodes, where σ denotes the standard deviation. Aged and H_2O samples show a greater variation in phase fraction, meaning the phase composition has a greater variance as a function of distance from the electrolyte.

σ of Phase Fraction	Pore	LSM	YSZ
Un-Aged	2.51	2.24	2.83
Aged in Air	3.75	5.45	2.61
Aged in H_2O	6.73	5.92	3.92

We note an interesting effect that was observed in the H_2O aged sample by the FEI ChemiSTEM system. As can be seen in Fig. 4, elemental maps were collected from a

collection of connected YSZ grains. Besides the expected Y and Zr signals, a significant amount of La and Mn was detected, primarily at the interfaces between the YSZ grains. This was highly unexpected, and suggests the possibility of LSM (or a similar phase) segregating preferentially to the grain boundaries of YSZ during operation with water present.

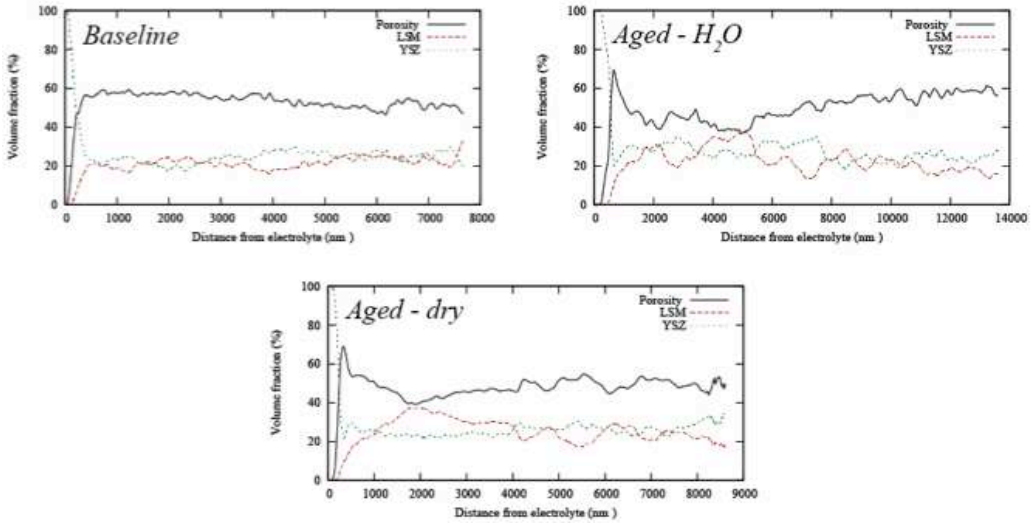

Figure 3. Plot of phase volume fraction as a function of distance from cathode/electrolyte interface. Samples aged in air and H_2O show greater deviation in phase fraction.

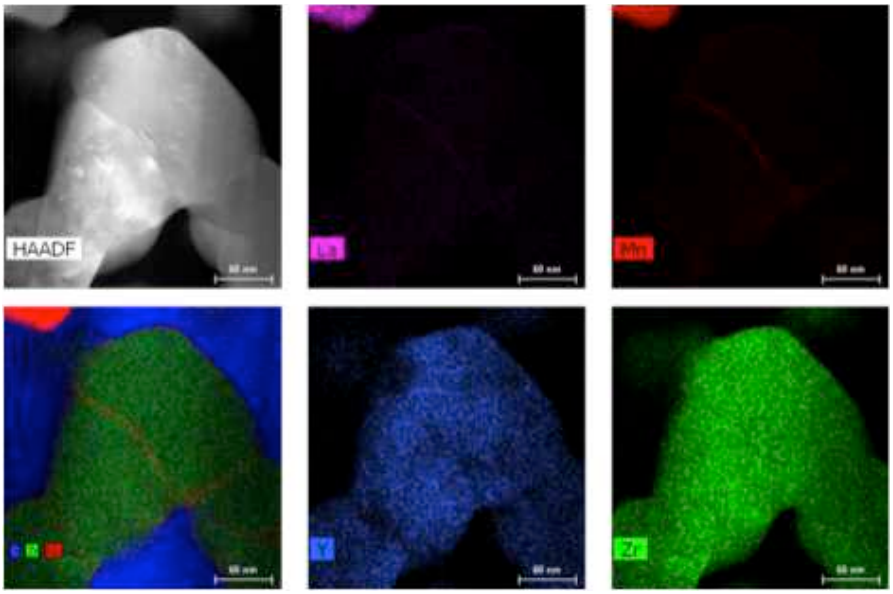

Figure 4. High-resolution STEM-EDS collection on a few agglomerated YSZ grains in the cathode. Data is taken from H_2O-exposed sample. The enhanced presence of La and Mn at the YSZ grain boundary suggests the possibility of phase segregation in the aged sample, warranting further evaluation. This effect has to this point not been observed in any other sample. Images collected on an FEI Titan™ G2 80-200 ChemiSTEM, courtesy of FEI Company.

LSM-YSZ/YSZ/LSM-YSZ Symmetric Cell in H_2O with Polarization

Figure 5 shows impedance plots of the Temperature-PO_2 dependence for an LSM-YSZ/YSZ/LSM-YSZ symmetrical cell at temperatures ranging from 700°C to 850°C. All measurements were taken under OC conditions, in symmetrical environments, using a two-electrode four-wire configuration, in which the entire resistance of the symmetrical cell is measured. We therefore expect the impedance contribution of a single composite cathode to be only half of what is measured. Effects of temperature and oxygen partial pressure can be clearly seen in Fig. 5. First, as temperature increases there is a decrease in both series and polarization resistance, R_S and R_P, respectively. The series resistance can be mostly attributed to the resistance of the electrolyte and is almost solely a function of temperature, although, as temperatures exceed 800°C there is a small decrease in Rs when flowing 100 SCCM N_2. The polarization resistance, R_P, is also a function of temperature, and decreases as temperature increases. This polarization resistance can be broken down into what seem to be three distinct arcs. The first arc appears to have a 45° slope leading into a semicircular arc, a characteristic that is distinctive of the Gerischer type component, usually associated with composite based cathodes. This first, high frequency arc, seems to shrink as temperature increases, but remains relatively constant with regard to changes in PO_2.

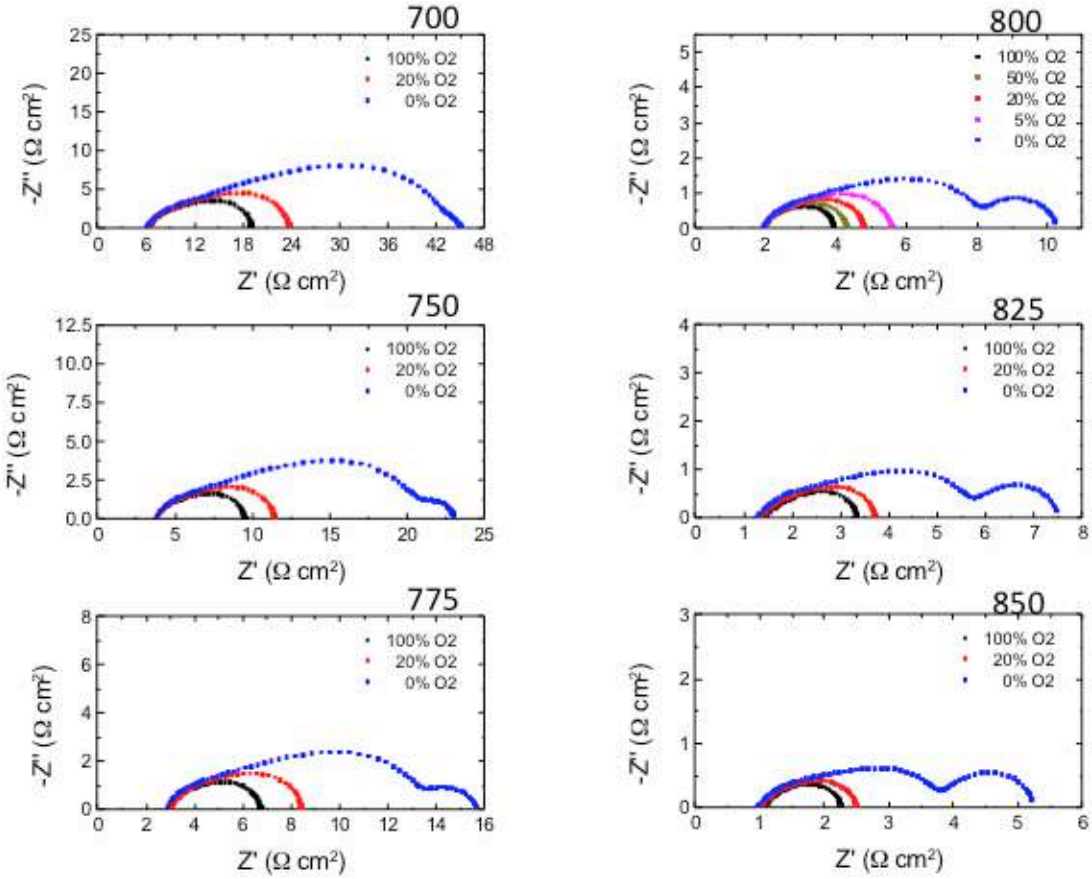

Figure 5. Impedance plots of LSM-YSZ/YSZ/LSM-YSZ symmetric cell under various PO_2 conditions at temperatures ranging from 700°C to 850°C. The presence of three separate arcs becomes apparent by varying the test conditions.

A second, medium frequency arc that is less apparent at high temperature and high PO_2, appears to shrink as temperature increases, similar to the high frequency arc, but has a much greater dependence on changes in PO_2. It can be seen readily in 800°C measurements shown in Fig. 5. As the PO_2 level decreases, there is a significant change in the size of this second arc. As such, we would also consider this arc to be a contribution of the electrode, possibly relating to the ORR. Finally, there is a third, low frequency arc, that only appears under the lowest PO_2 conditions, where 100 SCCM of N_2 is flowing across the cells cathodes (10^{-6} atm O_2). This is believed to be a caused by gas diffusion limitations when the presence of gas phase oxygen is scarce. Interestingly, the size of this low frequency arc increases, in relation to the high and medium frequency arcs, indicating that as temperature increases the gas-diffusion limitation under low PO_2 conditions becomes a limiting factor for performance. Figure 6 shows an Arrhenius plot of the effect of PO_2 on the area specific resistance (ASR) of the LSM-YSZ/YSZ/LSM-YSZ cell at 800°C. The slope of the log PO_2 vs log(ASR) double log plot is -0.11 describing, in qualitative terms, the PO_2 dependence of the cathode. This PO_2 dependence could potentially be used to qualify the oxygen species that are involved in the ORR by measuring the change of the PO_2 dependence with the presence of H_2O.

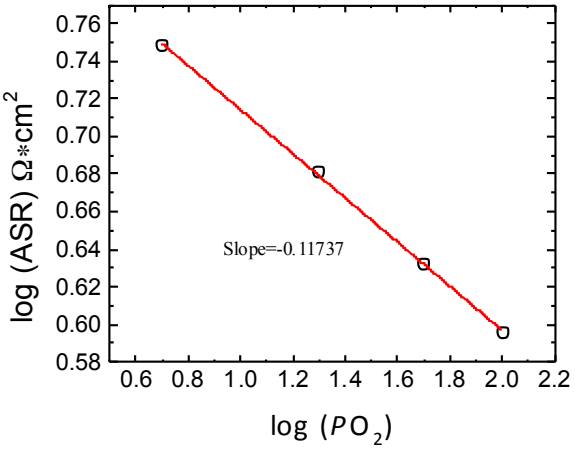

Figure 6. Arrhenius plot of log(ASR) vs. PO_2 of the polarization resistance at 800°C, identifying the PO_2 dependence of R_P for the LSM-YSZ/YSZ/LSM-YSZ symmetric cell.

Figures 7(a) and 7(b) are Arrhenius plots of log(ASR) vs. 1000/T for R_S and R_P, respectively. The slope of the fitted curve for R_S in Fig. 7(a) is 5.86, representing the temperature dependence of the series resistance of the symmetrical cell. On the other hand, Fig. 7(b) shows the dependence of R_P on changes in PO_2 as a function of temperature. This apparent activation energy could potentially be used to quantify physical or chemical degradation mechanisms by measuring the PO_2 dependence before and after exposure to contaminants, such as H_2O. We can see that the slopes for the fit lines for the various R_P values are all greater than the 5.86 calculated for R_S, indicating that the polarization resistance of LSM-YSZ composite cathode has a greater dependence on temperature than the bulk YSZ electrolyte. Going further, Fig. 7(b) shows how the temperature dependence of R_P changes under various PO_2. We can see from the plot that as the oxygen partial pressure decreases the total polarization resistance increases, as well as the slope of the fit line. Under a flow of 100 SCCM O_2 a slope of 6.82 has been calculated for R_P as a function of temperature, while values of 7.17 and 7.95 have been calculated for 80+20 SCCM, N_2+O_2 mixture, and 100 SCCM N_2, respectively.

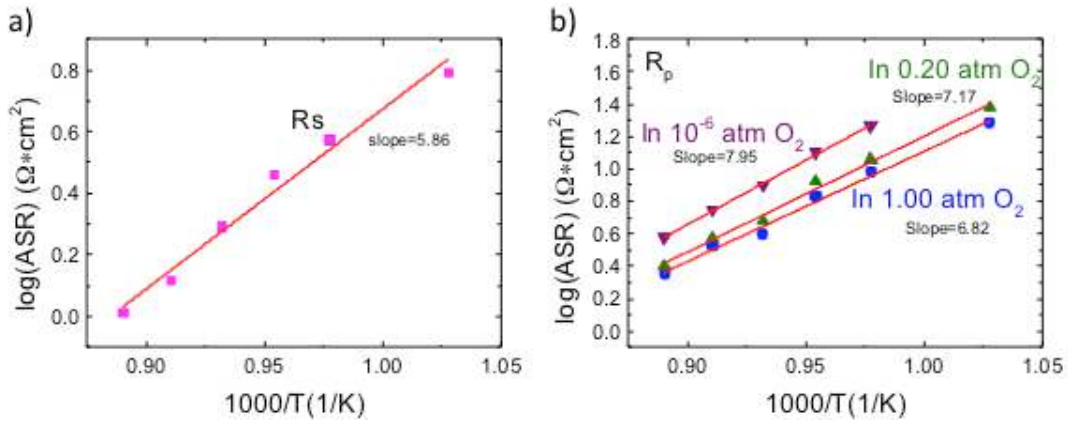

Figure 7. Arrhenius plot of log(ASR) vs. 1/T shows the apparent activation energy of (a) the series resistance R_S and (b) the polarization resistance R_p at different oxygen partial pressures.

Figure 8 shows impedance plots for an LSM-YSZ/YSZ/LSM-YSZ symmetrical cell measured under the cycling of applied bias and open circuit conditions in an H_2O environment over the course of 500 hours. Figure 8(a) shows measurements taken at 0, 80, and 140 hours in open circuit conditions, while Fig. 8(c) shows the impedance measurements taken after two hours of applied bias conditions over that same time period. Hours 200 to 500 are separated from the first 140 due to measurement errors occurring in that time period. As such, Fig. 8(b) and (d) show the impedance measurements taken between 200 and 500 hours of aging for OC and applied bias conditions, respectively. As can be seen in Fig. 8(a) and (c), there is a fast decrease in resistance over the first 140 hours. This trend can be better seen in Fig. 9(a) and (c), the ASR of the series (R_s), polarization (R_P) and total (R_T) resistances as a function of time for OC and applied bias conditions. Although the resistance trends for polarization and OC conditions seem to follow one another for the first 140 hours of aging, there appears to be a slight difference in the value of R_P between the two. A closer look at R_P (blue triangles) in Fig. 9(a) and (c) shows that during applied bias impedance measurements the values of R_P are higher. However, as the measurements continue beyond 140 hours, in the 200 to 500 hour range, the R_P values for the applied bias and OC impedance measurements become almost identical.

The insets of Fig. 8(b) and (d) show the result of stopping flow through water during the last 50 hours of the aging process. After bypassing the water bubbler there appears to be no significant change to the resistances measured during OC impedance. On the other hand, there seems to be a relatively sharp drop in the R_P values corresponding to impedance measurements with an applied bias. Further investigation may more accurately indicate which degradation mechanism is affected by the presence of water and applied bias.

In Figs. 2 and 9 we can see the trends for R_P as a function of time, where the prior is for a cell aged in an H_2O environment and the latter for a cell aged in H_2O with polarization. In Fig. 2 we a sharp decrease in the polarization resistance in the first ~50 hours, eventually leading to a slight increase over the next 340 hours. For the cell aged in H_2O with polarization we again see a sharper decrease in the value of R_P in the first ~50 hours, but the value of R_P continues to decrease over the next 450 hours. The decrease of R_P values for the composite cathode aged in H_2O under an applied bias could be an effect

of continued cathode particle coarsening and necking throughout the aging process. FIB-SEM analysis for the cells measured with an applied bias could help to clarify these results.

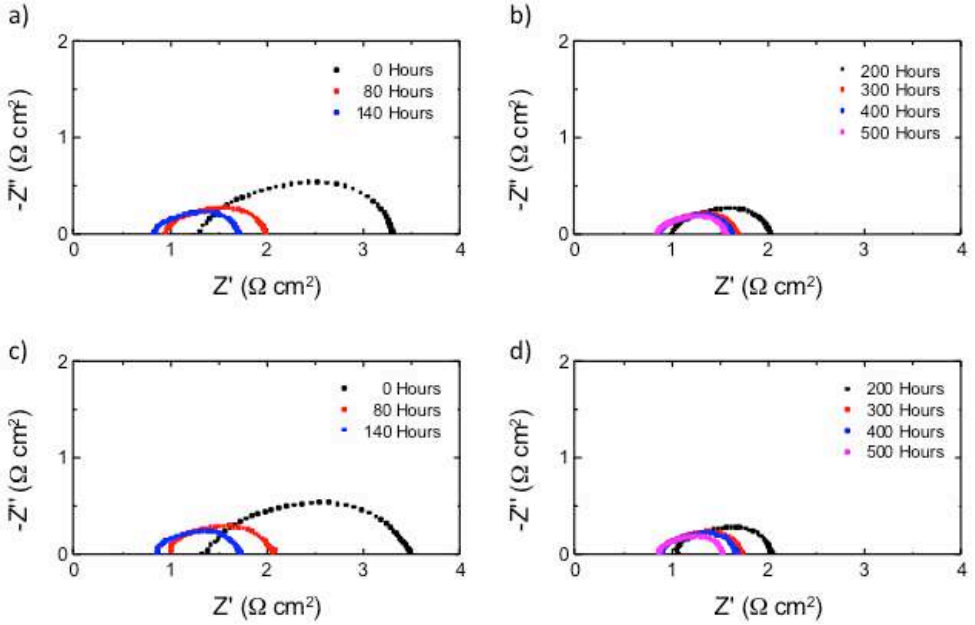

Figure 8. Impedance plots for the LSM-YSZ/YSZ/LSM-YSZ symmetric cell measured under (a)(b) open circuit and (c)(d) -0.7V applied bias conditions in an H_2O atmosphere, for (a)(c) 0 to 140 hours and (b)(d) 200 to 500 hours.

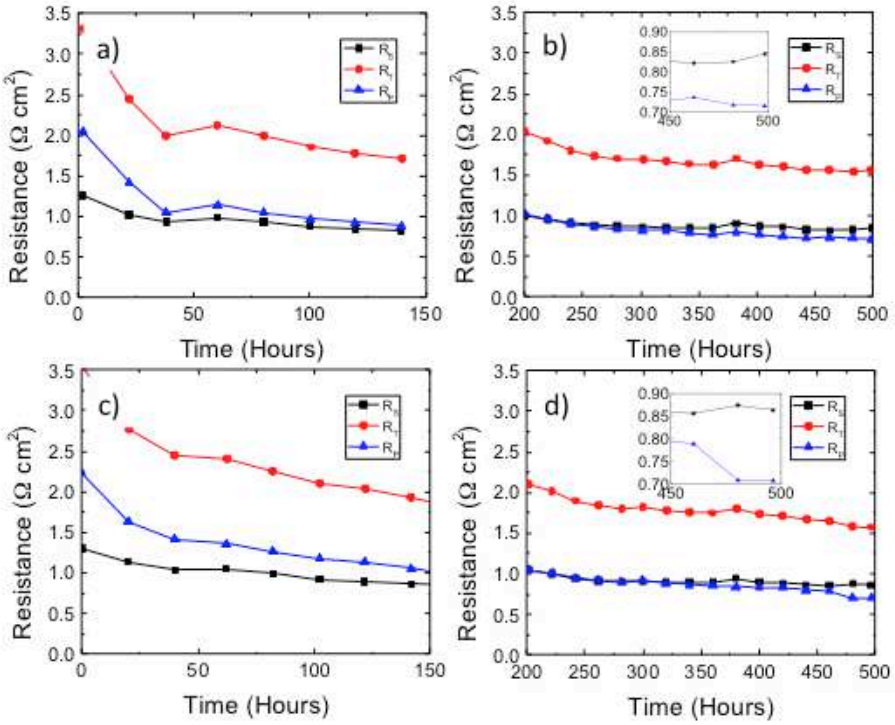

Figure 9. Resistance vs. time for the LSM-YSZ/YSZ/LSM-YSZ symmetric cell measured under (a)(b) open circuit and (c)(d) -0.7V applied bias conditions in an H_2O atmosphere, for (a)(c) 0 to 140 hours and (b)(d) 200 to 500 hours.

Conclusions

The durability of LSM-YSZ based cathodes in moisture has been studied though a multi-faceted investigation. LSM-YSZ/YSZ/LSM-YSZ symmetrical button cells were electrochemically tested under various PO_2 and temperature conditions by the *in-situ* EIS measurements. In addition these cells have been aged for over 380 hours in H_2O, with open circuit and -0.7V applied bias. Trends in polarization resistance, obtained through impedance spectroscopy, have been seen for the cell aged in H_2O under open circuit and correlated with isotope exchange data for powders tested in H_2O environments for equivalent time lengths. Post FIB-SEM and TEM results have been analyzed and indicate that cells exposed to H_2O environments at open circuit shows a coarsening of the microstructure as well as a migration of Mn atoms to YSZ grain boundaries. Combining these analysis techniques provides a clearer picture of the moisture effect on the degradation in different scales, from the micron scale 3D reconstruction to the nano scale kinetic reactions. Further analysis is needed to determine the rate at which these mechanisms occur, and their effect, if any on the overall performance of the cathode.

Symmetrical cells tested using 2-electrode impedance measurements have shown three arcs corresponding to various cathode mechanisms. The high frequency arc appears to be indicative of a Gerischer component, and has a strong temperature dependence, and is relatively unaffected by changes in PO_2. The medium frequency arc appears to be the result of an electrode effect and has a similar temperature dependence to the high frequency arc, but is affected much more to changes in PO_2. Finally the low frequency arc, attributed to gas diffusion limitations, appears only under low PO_2 conditions and has a lesser temperature dependence than the previous two arcs. Arrhenius plots for the dependence of cell resistance have been created, and slopes calculated. These slopes indicate the relationship between polarization resistance and temperature under various PO_2 conditions and could be crucial in distinguishing different electrode degradation contributions and how they change after aging in contaminant environments, helping to quantify if/how each degradation mechanism contributes to the overall cathode polarization.

Acknowledgments

The authors would like to acknowledge the support of the U.S. Department of Energy, SECA, Contract #: DEFE0009084. FIB-SEM analysis was performed in part at the NIST Center for Nanoscale Science and Technology. The authors would also like to acknowledge FEI Company for TEM images and analysis.

References

1. S. J. Benson, D. Waller, and J. A. Kilner, *J. Electrochem. Soc.*, **146**, 1305-1309 (1999).
2. D. Oh, D. Gostovic, E. D. Wachsman, *J. Mater. Res.*, **27,** 1993-1999 (2012).
3. Z. Zhao, L. Liu, X. Zhang, W. Wu, B. Tu, D. Ou, M. Cheng, *J. Power Sources*, **222**, 542-553 (2013).
4. B. C. H. Steele, *Solid State Ionics*, **86–88**, 1223-1234 (1996).
5. J. Nielsen, M. Mogensen, *Solid State Ionics*, **189**, 74–81 (2011).
6. J. Nielsen, L. A. Hagen, Y. L. Liu, *Solid State Ionics*, **181**, 517-524 (2010).

7. Z. Zhao, et al., *J. Power Sources*, **222**, 542-553 (2013).
8. E. P. Murray, T. Tsai. S. A. Barnett, *Solid State Ionics*, **110**, 325-243 (1998)
9. M. J. Jørgensen, S. Primdahl, M. Mogensen, *Electrochem. Acta*, **44**, 4195-4201 (1999)
10. M. J. Jørgensen, M. Mogensen, *J. Electrochem. Soc.*, **148**, A433-A442 (2001)
11. E. D. Wachsman, *Solid Oxide Fuel Cells X, ECS Transactions*, K. Eguchi, S. C. Singhal, H. Yokokawa, and J. Mizusaki, Ed, **7-1**, 1051-1054 (2007).
12. D. Gostovic, J. R. Smith, K. S. Jones and E. D. Wachsman, *Electrochem. Solid-State Lett.*, **10**, B214-217 (2007).
13. J. R. Smith, A. Chen, D. Gostovic, D. Hickey, D. Kundinger, K. L. Duncan, R. T. DeHoff, K. S. Jones and E. D. Wachsman, *Solid State Ionics*, **180**, 90-98 (2009).
14. D. Gostovic, N. J. Vito, K. A. O'Hara, K.S. Jones, and E. D. Wachsman, *J. American Ceram. Soc.*, **94**, 620-627 (2011).
15. J. R. Wilson, et al., *J. Power Sources*, **195**, 1829-1840 (2010)
16. J. Joos, T. Carraro, A. Weber, E. Ivers-Tiffée, *J. Power Sources*, **196**, 7302-7307 (2011)
17. J. Joos, M. Ender, T. Carraro, A. Weber, E. Ivers-Tiffée, *Elctrochem. Acta*, **82**, 268-276 (2012)
18. C. C. Kan and E. D. Wachsman, *J. Electrochem. Soc.*, **156**, B695-B702 (2009).
19. C. C. Kan and E. D. Wachsman, *Solid State Ionics*, **181**, 338-347 (2010).
20. E. N. Armstrong, K. L. Duncan, D. J. Oh, J. F. Weaver, and E. D. Wachsman, *J. Electrochem. Soc.*, **158**, B492-B499 (2011).
21. E. N. Armstrong, K. L. Duncan, and E. D. Wachsman, *J. Electrochem. Soc.*, **158**, B283-B289 (2011).
22. R. A. De Souza, J. A. Kilner, J. F. Walker, *Materials Letters*, **43**, 43-52 (2000)
23. D. V. Ivanov, E. M. Sadovskaya, L. G. Pinaeva, L. A. Isupova, *J. Catalysis*, **267**, 5-13 (2009)
24. Y. L. Huang, C. Pellegrinelli, E. D. Wachsman, *ECS Trans.*, **61**, 93-107 (2014)
25. J. A. Taillon, C. Pellegrinelli, Y. L. Huang, E. D. Wachsman, L. G. Salamanca-Riba, *ECS Trans.*, **61**, 109-120 (2014)